 doi:10.20944/preprints202206.0102.v1

Article

MiWEndo: Evaluation of a Microwave Colonoscopy Algorithm for Early Colorectal Cancer Detection in Ex Vivo Human Colon Models

Marta Guardiola [1,*], Walid Dghoughi [1], Roberto Sont [1], Alejandra Garrido [1], Sergi Marcoval [1], Luz María Neira[1], Ignasi Belda[1] and Glòria Fernández-Esparrach [1,2]

[1] MiWEndo Solutions S.L., 08014 Barcelona, Spain.
[2] Endoscopy Unit, Gastroenterology Department, Hospital Clínic, University of Barcelona. CIBEREHD. IDIBAPS, 08036 Barcelona, Spain; mgfernan@clinic.cat.
* Correspondence: Marta Guardiola; marta@miwendo.com

Abstract: This study assesses the efficacy of a microwave colonoscopy algorithm to detect colorectal cancer precursors or polyps in an ex-vivo human colon model. The algorithm works with a device composed of a cylindrical ring-shaped switchable antenna array, which can be attached to the tip of a conventional colonoscope as an accessory. The accessory is connected to an external processing unit that generates an acoustic signal when a polyp is detected. Nowadays, 22% of polyps go undetected with conventional colonoscopy and the risk of cancer after a negative colonoscopy can be up to 7.9%. Fifteen ex-vivo freshly excised human colons with cancer (n=12) or polyps (n=3) were examined with the microwave-assisted colonoscopy system simulating a real colonoscopy exploration. Successive measurements of the colon were taken with the microwave-based colonoscopy device and processed with a microwave imaging algorithm. After the experiment, the dielectric properties of the specimens were measured with a coaxial probe and finally the samples underwent a pathology analysis. The results show that all the neoplasms were detected with a sensitivity of 100% and specificity of 87.4%.

Keywords: endoscopes; medical diagnostic imaging; microwave antenna arrays; microwave imaging; colorectal cancer

1. Introduction

Colorectal cancer (CRC) is a major health and economic burden in the context of an increasingly aging population. Globally, 1.93 million new cases of CRCs are diagnosed annually, and 935,000 people died in 2020 [1], making CRC the second most common cause of cancer death in both men and women. CRC is a malignant disease that affects the colon and rectum. 90% of CRCs start off as a polyp, an abnormal colon mucosa growth [2]. Although some polyps are harmless, the type called adenoma is premalignant and slowly become cancerous. Polyps are usually asymptomatic or present mild symptoms. Due to this, with the current diagnosis methods, CRC is commonly found in advanced stages [3]. The overall five-year survival rate is approximately 65%, but it strongly depends on the development stage at diagnosis, dropping to 14% if cancer has spread to distant parts of the body. Fortunately, early diagnosis can dramatically improve prognosis, saving lives and reducing healthcare costs.

To date, colonoscopy is the most effective diagnostic and therapeutic technique for the prevention of colorectal cancer since it allows the identification and removal of polyps in the entire colon in a procedure called polypectomy. Several prospective studies demonstrate that colonoscopy with polypectomy reduces the incidence of CRC by 40–90% [4,5]. During a colonoscopy, a long, flexible tube called colonoscope is inserted into the rectum. A tiny video camera at the tip of the tube allows the doctor to view the inside of the colon. Nevertheless, colonoscopy is far from perfect: 22% of polyps go undetected [6] and the

Preprints (www.preprints.org) | NOT PEER-REVIEWED | Posted: 7 June 2022 doi:10.20944/preprints202206.0102.v1

risk of cancer after a negative colonoscopy is still 7.9% [7]. The main causes of this lack of efficacy are visualization limitations of the optical camera with a field of view typically less than 180° [8], inhomogeneous illumination, colon angulations and folds, and poor cleaning of the colon. For this reason, 13.4% of the colon surface area might not be visualized during a colonoscopy [9].

To solve this problem, several endoscopic devices and technologies have been developed to improve the adenoma detection rate (ADR). ADR is the quality indicator of colonoscopy, as each 1% increase in ADR decreases patients' risk of CRC by 3% [10]. High-definition endoscopes, endoscopes with multiple lenses, and mucosal flattening accessories [11,12], have demonstrated an increase in ADR of 4.5%, 5% and 16% respectively by improving the visualization [13]. Chromoendoscopy, endoscopic microscopy (endocytoscopy and endomicroscopy) or hyperspectral techniques [14] are methods developed to magnify and enhance mucosa tissue characteristics that can be linked to malignancy, but have failed to demonstrate significant increases in ADR [13]. All these techniques are restricted to the optical information captured by the camera and require highly trained professionals. Because the outcomes of these methods are highly dependent on operator's experience and human factor (fatigue, stress, resilience, etc.), a tool capable to automate the detection of polyps is needed. Artificial intelligence is increasingly used for real-time assessment of endoscopic images [15] showing an increase in ADR of 14% [16]. However, if the adenoma is not visualized by the camera, it cannot be detected by the algorithm.

We recently proposed microwave imaging, a non-ionizing, anatomical and functional imaging method [17] to detect polyps in the colon. Microwave imaging is based on retrieving the dielectric properties of a target −the relative permittivity and the conductivity− from the measured electromagnetic fields. The dielectric properties are biomarkers of several health conditions such as breast cancer [18,19], brain stroke [20], osteoporosis [21], heart infarction [22], or edema. With respect to advanced colonoscopy methods, microwave imaging offers a new contrast mechanism based on the dielectric properties of tissues. We demonstrated in an ex-vivo study with human colon polyps and healthy mucosa, that the dielectric properties of colon polyps increase when the malignancy grade increases. The contrast between healthy colon mucosa and colorectal cancer is 30% and 90% for the relative permittivity and conductivity, respectively, at 8 GHz [22]. We also have developed a prototype to integrate microwave imaging to conventional colonoscopy called MiWEndo. MiWEndo is a ring-shaped switchable antenna array accessory attachable to the distal tip of a standard colonoscope connected to an external processing unit. MiWEndo generates an acoustic signal when a polyp is detected using microwave imaging [23]. In contrast to artificial intelligence assisted colonoscopy, MiWEndo is not restricted to the information delivered by the optical camera, providing a wider field of view of 360°. Regarding the algorithm, a frequency domain reconstruction scheme based on a modified backprojection method preceded by a calibration was developed to form cross-sectional images every 4 mm for each colon model. For each image, a fixed threshold was used to detect if a polyp is present. A first version of the algorithm was tested in phantoms [24] and in ex-vivo models [25]. The conclusion of these studies was that the calibration and the detection steps had to be improved. In [26] we performed a comparative study between 5 different calibration methods to define the most suitable one.

In this paper we present an improved microwave colonoscopy algorithm for colorectal cancer early detection. The aim of this study is to assess the overall algorithm performance with 15 freshly excised human colon specimens with neoplastic lesions. This algorithm uses the calibration scheme identified in [26] and an improved automatic detection method. The colons were placed on a setup designed to emulate a colonoscopy exploration with the MiWEndo microwave-based colonoscopy system. The results have been compared with the gold standard pathology analysis in terms of sensitivity and specificity. We also characterized the dielectric properties of the specimens at 7.6 GHz with an open-ended coaxial probe.

Preprints (www.preprints.org) | NOT PEER-REVIEWED | Posted: 7 June 2022 doi:10.20944/preprints202206.0102.v1

2. Materials and Methods

2.1. Microwave-based colonoscopy system

The imaging system is composed of an external processing unit and an acquisition accessory. The external unit contains a vector network analyzer (VNA Keysight E5071C), a microcontroller (Arduino Nano), and a laptop. The acquisition accessory consists of a ring-shaped encapsulated switchable antenna array attached to the tip of a conventional colonoscope. The antenna array is composed of two rings of eight antennas, one containing the transmitting and the other the receiving antennas. The antenna elements are cavity-backed slot antennas operating over the 7.6-7.66 GHz range in free space. The reduced bandwidth is due to the miniaturization of the antennas, as described in a previous paper [23]. The antenna elements are welded onto a polyamide flexible printed circuit board (PCB) that contains the microstrip feeding lines and two single-pole-eight-throw (SP8T) radiofrequency switches. This assembly is wrapped around a 3D printed piece that adapts the PCB with the colonoscope. Finally, it is encapsulated with a biocompatible 3D printed resin to protect the PCB from moisture and to avoid injuring the colon mucosa tissue. The final dimensions of the accessory are 30 mm in length by 20 mm in diameter, exceeding the colonoscope's diameter by less than 3 mm. The dimensions and shape of the accessory device ensure non-obstruction of the colonoscope's front tip, maintain the maneuverability of the colonoscope, avoid camera concealment, and prevent injuries to the patient. Two slim 500 mm in length and 1.13 mm in diameter coaxial cables transmit the microwave signals, and eight wires transmit the switches' control signals. Miniature connectors are used for a non-bulky final assembly. Figure 1 shows the block diagram of the proposed MiWEndo system.

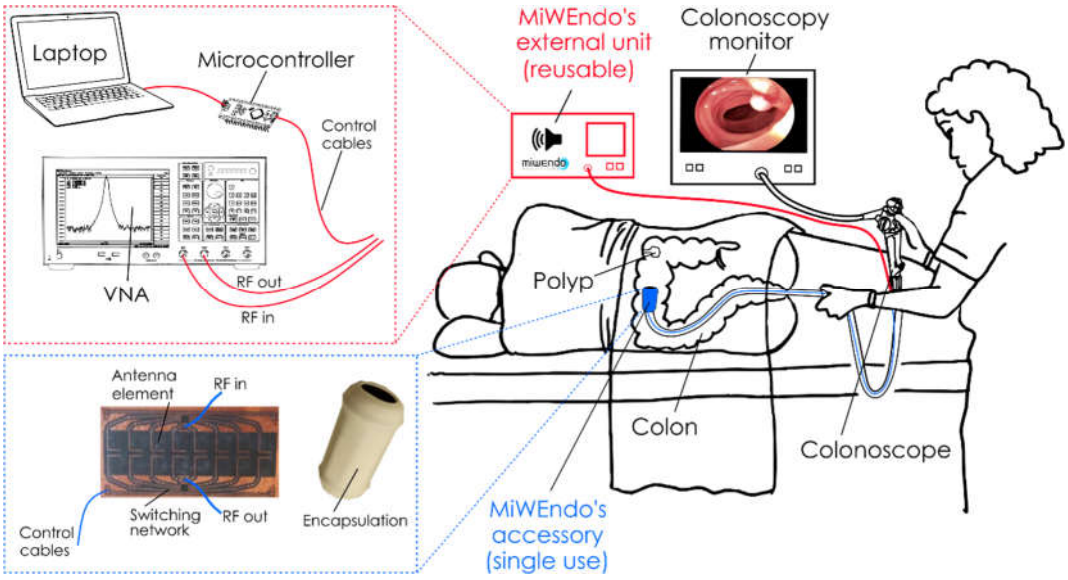

Figure 1. MiWEndo's microwave endoscopy system is composed by an accessory attachable at the distal tip of a standard colonoscope and an external processing unit. MiWEndo generates an acoustic signal when a polyp is detected to warn the endoscopist.

2.2. Setup for Ex-Vivo Human Colon measurements

The colon is the last part of the gastrointestinal tract. It has a segmented appearance due to a series of folds, and it is about 1,500 mm long and 40-90 mm in diameter. Polyps are slow-growing overgrowths of the colonic mucosa protruding into the lumen.

To reproduce a realistic colonoscopy exploration with ex-vivo colon fragments, we created a colon fixation setup and a positioning setup to move MiWEndo's accessory along the ex-vivo colon lumen shown in Figure 2 (a). The positioning setup was composed of a T-shaped metallic structure fixed on a plastic base. The metallic structure holds a plastic bar that simulates a colonoscope tube. MiWEndo's accessory is attached at the tip

Preprints (www.preprints.org) | NOT PEER-REVIEWED | Posted: 7 June 2022 doi:10.20944/preprints202206.0102.v1

of the plastic bar. With this bar, the accessory was introduced horizontally inside the ex-vivo colon lumen and was moved along it to obtain the measurements.

The 15 surgically excised human colon samples of at least 10 cm long containing cancer or polyps were scanned with the MiWEndo. Immediately after the excision, the fresh specimens were opened longitudinally by a clinician and then fixed around a tube of expanded polystyrene and wrapped with a soaker pad. Expanded polystyrene behaves like air for microwaves and therefore it has a minimal impact on the radiated electromagnetic fields. It represents a realistic situation since during a colonoscopy, the colon is expanded using carbon dioxide insufflation to increase colon visualization. The wrapped sample was placed on a platform with L-shaped plastic pieces to fix the sample during the procedure, and the platform was placed on a lifting platform to control the vertical position. Table 1 shows the characteristics of the human colon samples measured. Samples 11, 12 and 13 were wrapped around a curved polystyrene foam to model a more challenging situation that is a colon angulation. Moreover sample 12 presented a suboptimal cleaning of the colon with some debris along the mucosa.

After the exploration with MiWEndo's accessory, the dielectric properties of the colon mucosa and the neoplasm were measured using the open-ended coaxial probe method using the Keysight N1501A Dielectric Slim Form Probe Kit with the N1500A Materials Measurement Software Suite connected to a vector network analyzer Keysight E5071C. We performed three measurements on the neoplasm and three measurements on three equidistant locations on the healthy mucosa (start, center, and end). The different tissues were identified by a pathologist prior to the measurement with the coaxial probe. We followed the recommended procedure for obtaining high quality measurements with the open ended coaxial probe [27,28]. The setup is depicted in Figure 2 (b). The colon samples have been measured with the shortest possible cold ischemia time and without any conservation treatment (i.e., without formaldehyde) to preserve their physical and dielectric properties. Samples from patients that underwent previous radiation therapy or chemotherapy have been excluded. Finally, the specimens were sent to the Pathology Department for histological analysis of the neoplasms.

The study was conducted according to the guidelines of the Declaration of Helsinki and approved by the Institutional Review Board of Hospital Clínic de Barcelona (protocol code HCB/2017/0519 and date of approval 06/29/2017). Informed consent was obtained from all subjects involved in the study.

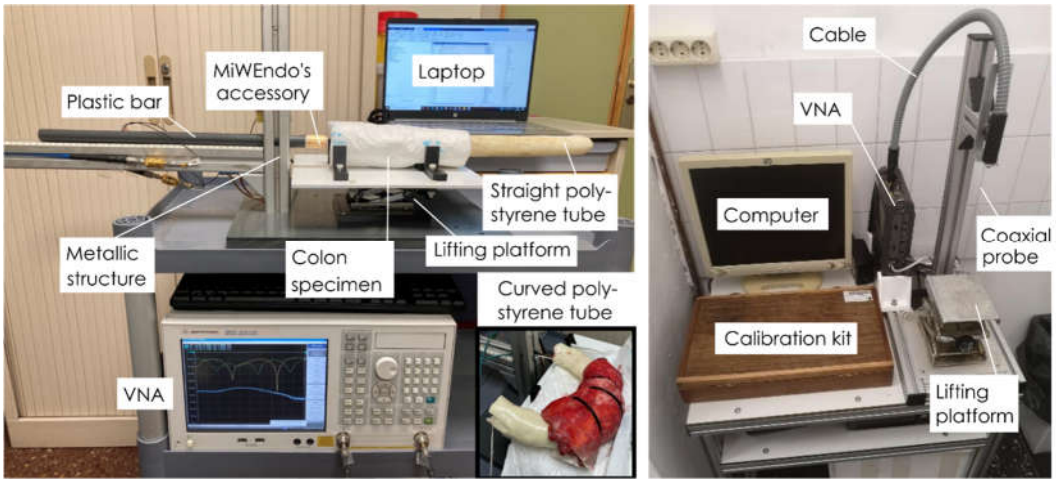

(**a**) (**b**)

Figure 2. Setup for ex-vivo human colon measurements: (**a**) Setup for the exploration of ex-vivo human colon samples with MiWEndo's accessory; (**b**) Setup for measuring the dielectric properties of ex-vivo colon samples with the open-ended coaxial probe method.

Preprints (www.preprints.org) | NOT PEER-REVIEWED | Posted: 7 June 2022 doi:10.20944/preprints202206.0102.v1

2.3. Polyp detection algorithm for microwave-assisted colonoscopy

The MiWEndo's accessory was moved inside the colon model in a straight trajectory throughout the center of the lumen to simulate a colonoscopy exploration for polyp detection. A microwave image of a cross-section of the colon (XY plane) was obtained for each step in the trajectory, which was performed in 4 mm increments along the z-axis. Figure 3 presents the geometry of the imaging setup. Each step in the trajectory and its microwave image is referred to as a frame, being n the index of the current frame.

The data for creating the microwave image at each frame is obtained by subsequently illuminating the colon tissue with a microwave signal radiating from a transmitting antenna and measuring the total field at the three receiving antennas that are closest to the transmitting one (the adjacent antenna and the two diagonal antennas). The measured total field results from the interaction of the incident microwaves and the colon tissues and therefore contains information about the spatial distribution of the dielectric properties of the colon. The process is repeated for each of the 8 transmitting antennas to scan the entire perimeter of the colon. In total, 24 combinations of transmission S-parameters are measured and used to produce the microwave image the frame's cross-sectional slice of the colon.

The microwave image reconstructions were obtained at a single frequency of 7.6 GHz corresponding to the center frequency of the antennas. Since the antennas are narrowband, using more frequencies within their bandwidth does not provide additional independent information for reconstruction.

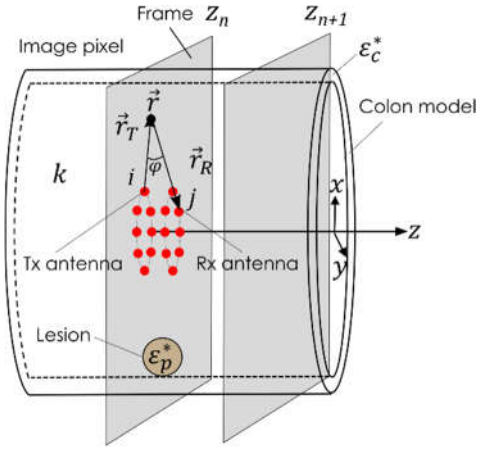

Figure 3. Geometry of the imaging problem.

A three-step algorithm is used to obtain the output, i.e., the acoustic signal when a polyp is detected, for each measured frame n.

2.3.1. Calibration

The aim of the calibration step is to clean the total field of unwanted effects including: the unknown distance to the colon walls, the colon folds, the angulations, etc., and to keep the response due to the presence of the polyp. Automatic Temporal (AT) subtraction calibration relies on the hypothesis that the impact on the scattered field that is caused by a polyp is much more important than the one produced by any other of the previously mentioned effects. Hence, for each frame, this strategy identifies the most similar frame to the current one and subtracts them. By doing so, the only effect that would remain after the calibration is the polyp response. The similarity between frames is computed using the Modified Hausdorff Distance, whose potential as S-parameters similarity measurer has been already proved [29].

Preprints (www.preprints.org) | NOT PEER-REVIEWED | Posted: 7 June 2022 doi:10.20944/preprints202206.0102.v1

2.3.2. Focuser

Once the data is calibrated, a Modified Monofocusing algorithm [30] is applied to obtain an image of the dielectric contrast profile $I_{z_n}(\vec{r})$:

$$I_{z_n}(\vec{r}) = \left| \sum_{j=(i-1)_{N_a}}^{(i+1)_{N_a}} \sum_{i=0}^{N_a-1} E_s^2\left(\vec{r}_{T_i}, \vec{r}_{R_j}, z_n\right) J_1^2\left(k\left|\vec{r}_{R_j} - \vec{r}\right|\right) e^{j2(k\left|\vec{r}_{R_j}-\vec{r}\right|+\varphi)} \right| \quad (1)$$

Being $k = 2\pi cf$ the wavenumber, and φ the angle between the transmitting and the receiving antennas, and E_s the scattered electric field. This Focuser method provides the image of the dielectric contrast profile. c is the speed of light since the colon is insufflated with carbon dioxide during the procedure.

2.3.3. Detector

The detection method implemented is based on a forecasting exponential smoothing method for detection of outliers [31,32]. We have observed that high amplitudes in the microwave images usually correspond to the presence of a polyp, but the high amplitude values are not comparable between different trajectories (different colon specimens). Therefore, we can detect the presence of a polyp by finding outlying values of the maximum amplitude of the reconstructed microwave image compared to previous frames in the same trajectory.

The first step in the detection algorithm is to compute an estimate of the maximum amplitude of the image for the next frame, $s(n+1)$, based on the previous estimation of the current frame and its actual maximum amplitude, $y(n)$ as follows:

$$s(n+1) = \alpha * y(n) + (1-\alpha) * s(n) \quad (2)$$

Where α is a constant between [0, 1]. The next step is to compute the confidence band b in which the next maximum amplitude of the image will likely lie.

$$b(n+1) = s(n+1) \pm [\alpha * [y(n) - s(n)] + (1-\alpha) * b(n)] * \delta \quad (3)$$

Here δ is a constant higher than 1. When the maximum reconstructed amplitude of the analyzed frame lies above its confidence band, the algorithm concludes that a polyp is detected and activates the acoustic signal.

3. Results

3.1. Sample characterization results

Using the data provided in the pathology report, we identified and labeled all the measured frames: healthy mucosa, adenomas with high grade dysplasia (HGD) and adenocarcinomas. Note that high grade dysplasia refers to precancerous changes in the cells. Table 1 summarizes the main characteristics of the 15 colon examinations, and Figure 4 shows the relative permittivity and conductivity of the healthy colon mucosa and neoplasm of each patient. If we look at the dielectric properties of each patient individually, we see that the dielectric properties of the neoplasm are always higher than those of the healthy mucosa. However, there is considerable variability between patients. This makes it impossible to establish a threshold that allows differentiating the healthy mucosa and the neoplasm for all patients. It is worth mentioning that accurately measuring the dielectric properties of healthy mucosa is very difficult since it is a very fine tissue, between 0.5 and 2 mm. Moreover, the part opposite the lumen was covered with very variable amounts of fat. Since we could not manipulate the samples so as not to alter the subsequent pathological analysis, the uniformity of the samples cannot be guaranteed. So, part of the variability between patients could be attributed to this issue.

Preprints (www.preprints.org) | NOT PEER-REVIEWED | Posted: 7 June 2022 doi:10.20944/preprints202206.0102.v1

Table 1. Characteristics of the trajectories measured in human colon models and performance evaluation of the implemented algorithm in terms of sensitivity and specificity.

Patient	Age	Type of neoplasm	Neoplasm size (mm)	Sample length (mm)	Sensitivity (%)	Specificity (%)
1	86	Adenoma with HGD[1]	10	200	100	80
2	64	Adenocarcinoma[2]	50	220	100	94.12
3	46	Adenocarcinoma	36	80	100	100
4	37	Adenoma with HGD	32	155	100	87.50
5	83	Adenocarcinoma	48	190	100	90.91
6	60	Adenocarcinoma	37	190	100	77.78
7	57	Adenocarcinoma	65	330	100	88.37
8	68	Adenocarcinoma	15	320	100	85.71
9	86	Adenoma with HGD	23	270	100	86.54
10	85	Adenocarcinoma	34	285	100	87.23
11	45	Adenocarcinoma[3]	32	260	100	83.33
12	75	Adenocarcinoma[4]	35	180	100	86.36
13	91	Adenocarcinoma[3]	40	160	100	84.21
14	62	Adenocarcinoma[3]	37	228	100	92.86
15	81	Adenocarcinoma	63	97	100	100

[1]HGD means high grade dysplasia and refers to precancerous changes in the cells. [2]Adenocarcinoma is a cancer that begins in glandular cells. [3]Curved trajectories emulating a colon fold. [4]Trajectory with a suboptimal colon cleaning.

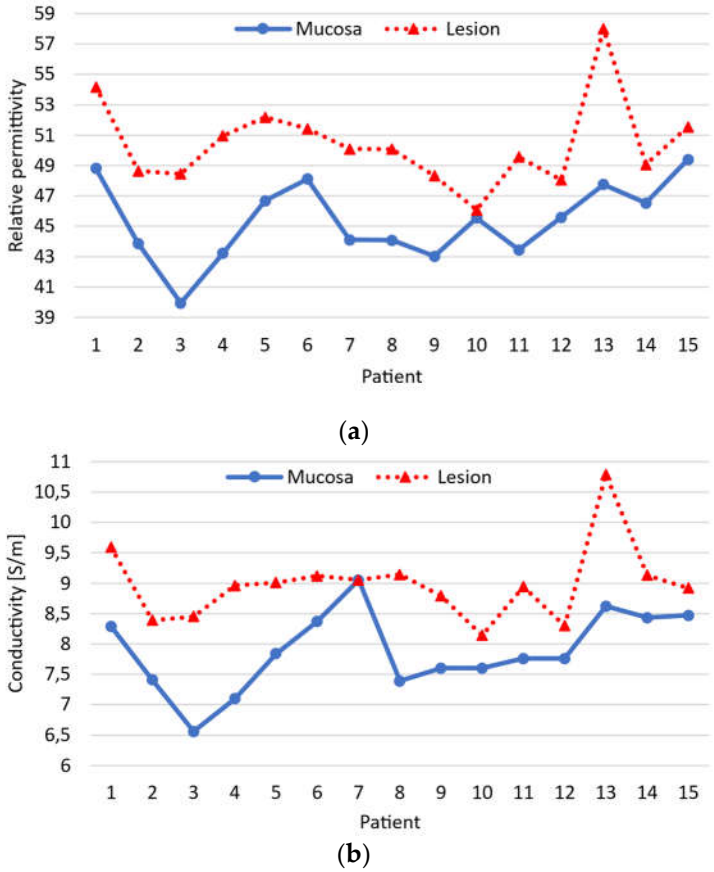

Figure 4. Dielectric properties of the healthy colon mucosa and the neoplasm at 7.6 GHz for each patient obtained with an open-ended coaxial probe. (**a**) Relative permittivity, (**b**) conductivity.

Preprints (www.preprints.org) | NOT PEER-REVIEWED | Posted: 7 June 2022 doi:10.20944/preprints202206.0102.v1

3.2. Polyp detection results

Following data acquisition and processing, the results of the microwave-based colonoscopy were obtained. The performance of the method to detect polyps in a trajectory is evaluated using the sensitivity and specificity. The sensitivity, also called the true positive (TP) rate, measures the percentage of cases having a polyp that are correctly diagnosed as having the lesion. A false negative (FN) occurs when a negative result is reported to a trajectory that does have a polyp. The specificity, also called the true negative (TN) rate, measures the percentage of healthy cases that are correctly identified as not having any polyp. A false positive (FP) is reported when the test wrongly indicates that a polyp is present. The values of sensitivity and specificity are related to TP, FP, TN, and FN values as follows.

$$\text{Sensitivity (\%)} = \frac{\text{TP}}{\text{TP} + \text{FN}}, \qquad \text{Specificity (\%)} = \frac{\text{TN}}{\text{TN} + \text{FP}} \tag{4}$$

Table 1 shows that in all the 15 cases the neoplasm has been detected with microwave-based colonoscopy. The overall sensitivity is 100% and the specificity is 87.43%.

As an example, Figure 5(**a**) shows the evolution of the maximum amplitude of the reconstructed image registered in each step of the trajectory. Figure 5(**c**) presents the maximum amplitude of the microwave image in front of each pair of antennas, and here moreover, it is possible to observe that the impact of the lesion is much more significant on the antennas 0-7,0,1 (transmitter 0 and receivers 7, 0 and 1), which are the ones that are facing the neoplasm.

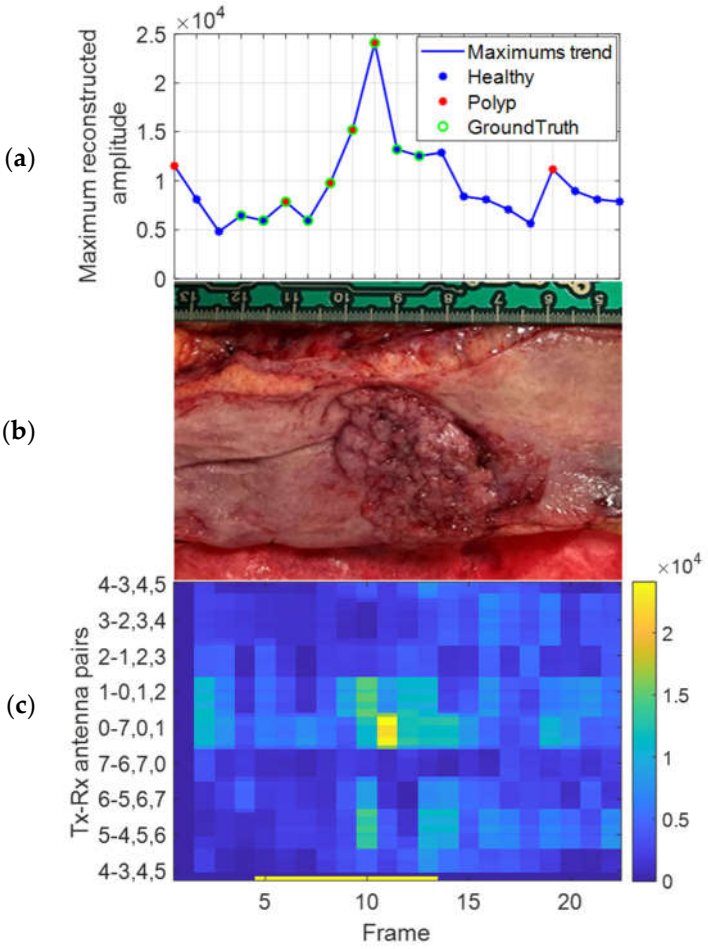

Figure 5. Results of patient 4. (**a**) Evolution of the maximum amplitude of the reconstructed image for each frame of the trajectory, (**b**) photograph of the colon sample with an adenoma with HGD, (**c**) maximum amplitude in front of all the antenna combinations.

Preprints (www.preprints.org) | NOT PEER-REVIEWED | Posted: 7 June 2022 doi:10.20944/preprints202206.0102.v1

4. Discussion

Missed lesions at colonoscopy are as high as 22% and have important clinical consequences. In the last years, many efforts have been made to improve the performance of endoscopy, but the common limitation of these methods is that they cannot detect what is not displayed by the camera.

In this study we have shown that the improved version of the algorithm is able to detect neoplastic lesions in human colon models. To do so, the MiWEndo microwave colonoscopy accessory device attached to a colonoscopy simulating setup was used. The system can detect neoplastic lesions on the full perimeter of the colon based on the changes in their dielectric properties and may be used to complement the endoscopic image. The system has been designed to be compatible with colonoscopy, ensure a full coverage and produce minimal changes to the current clinical practice. The final dimensions of the acquisition accessory device are 30 mm in length by 20 mm in diameter, having a total thickness of 3 mm. The dimensions and shape of the device ensure non-obstruction of the front tip of the colonoscope, avoiding injuring the patient or hindering the maneuverability of the colonoscope. The antennas work at 7.6 GHz over a narrow bandwidth and with an acceptable coupling.

A frequency domain imaging reconstruction algorithm based on Fourier backprojection preceded with an Automatic Temporal subtraction calibration has been developed to obtain cross sectional images of the colon. An automatic detection step based on exponential smoothing has been applied to obtain an output easy to interpret by the physicians, i.e., and acoustic alarm, when a polyp is detected. This kind of output has been inspired by the acoustic parking system for automobiles. The system provides an audible warning with a series of beeps as the car, or the endoscope, moves nearer a stationary object, or a polyp. The algorithm is fast and able to work in real time delivering around 10 frames/s. In terms of performance, the algorithm has reached a sensitivity of 100% and a specificity of 87.43%. No significant degradation of performance has been observed when the trajectory is not straight (trajectories 11, 13 and 14). This may indicate that the algorithm, and especially the calibration, can deal with the angulations of the colon. Debris in the colon (trajectory 12) has not degraded performance either. In the absence of further validation and if this is confirmed in future tests, it could be studied whether microwave-assisted colonoscopy could reduce the need for colon preparation. The impact of poor preparation is important since it forces to repeat the colonoscopy. In addition, the preparation required for the patient to clean the colon is the most uncomfortable part of the colonoscopy according to patients. It is worth mentioning that by changing the value of the constants α and δ used in the exponential smoothing method it is possible to tune the sensitivity and specificity values. We decided to force an optimal sensitivity because our device is aimed to prevent polyps from being missed once combined with colonoscopy. A suboptimal sensitivity can be accepted because our device is used in conjunction with the colonoscope. In case the acoustic signal is heard, the finding will always be confirmed with the video from the colonoscope.

Regarding the dielectric and pathologic characterization of the lesions, at 7.6 GHz healthy colon mucosa and neoplastic lesions exhibit inter-patient contrast in dielectric properties that allow its differentiation. However, the variation between patients do not allow to fix a permittivity threshold to differentiate all the healthy and neoplastic tissues. This is not a problem for the MiWEndo's system since the detection criteria is defined for each patient.

The main limitation of this study is the low number of adenomas studied. The device was validated in ex-vivo human colons that usually are surgically resected because they have already developed cancer. These lesions are commonly big and are not representative of what is commonly found in a regular colonoscopy. The second limitation is that the real-time acquisition system has not been tested. In this study, a measurement was taken after each trajectory step manually. To make the acquisition in real time, a second generation of external unit is being developed. The last limitation is that the device was

 doi:10.20944/preprints202206.0102.v1

not attached at the end of a real endoscope and the maneuverability and safety could not be assessed. Safety must be guaranteed from two fronts: energy safety and mechanical safety. In terms of energy, we refer to limit the radiation to avoid any biological effect to the patient's mucosa, i.e., heating, but also ensure the electrical safety and electromagnetic compatibility. In terms of mechanical safety, the accessory device must be designed with smooth surface, using biocompatible materials in the parts that are in contact with the patient, and the materials must be clean, i.e., with low bioburden.

For all these reasons, we are developing increasingly realistic anatomic models with folds and polyps of different sizes and shapes made of materials that mimic the dielectric properties of colon tissues. In the phantoms we also can study different trajectories varying the distance between the antennas and the colon wall while controlling the ground truth, i.e., the position of the polyp. The results with the simplest phantom can be found in [24]. We are also planning new studies in animal models to check the maneuverability and the inter-compatibility with other endoscopic devices used in real explorations such as forceps or electrocautery tools.

5. Conclusions

This paper presents the algorithm validation of a microwave colonoscopy system with 15 ex-vivo human colons with neoplastic lesions. The system consists of an acquisition accessory attachable to the distal tip of a standard colonoscope connected to an external processing unit. The algorithm is composed of 3 steps: calibration, focusing and automatic detection. A sensitivity of 100% and a specificity of 87.43% has been achieved, indicating that the detection algorithm is able to deal with real human colon tissues. The algorithm was able to deal with colon angulations. This confirmed what we observed with phantoms, where a more realistic movement within the colon has been reproduced. This demonstrates that the calibration method can deal with the changing distances between the antennas and the colon wall. In one trajectory, the algorithm was able to detect the lesion even in suboptimal cleaning conditions.

We are currently carrying out a measurement campaign with a new phantom extracted from a 3D model of a real patient with angulations and folds. With this model, several trajectories will be measured with the accessory attached to a real colonoscope and the algorithm will be used in real time. This setup will allow to conclude the algorithm validation with more challenging conditions before starting the clinical phase.

Supplementary Materials: All data generated or analyzed during this study are included in this article. Further enquiries can be directed to the corresponding author.

Author Contributions: Conceptualization, M.G. and G.F.; methodology, M.G.; software, W.D., A.G. and L.N.; validation, M.G., R.S. and S.M.; formal analysis, M.G., W.D. and A.G.; investigation, M.G., W.D., A.G. and L.N.; resources, M.G. and G.F..; data curation, W.D. and A.G..; writing—original draft preparation, M.G.; writing—review and editing, M.G., W.D.; visualization, G.F.; supervision, M.G.; project administration, I.B..; funding acquisition, I.B. All authors have read and agreed to the published version of the manuscript.

Funding: This research was funded by the European Union's Horizon 2020 Research and Innovation Programme, grant number 960251 and by the Spanish Ministry of Science and Innovation, grant number DIN2019-010857/AEI/10.13039/501100011033.

Institutional Review Board Statement: The study was conducted according to the guidelines of the Declaration of Helsinki and approved by the Institutional Review Board of Hospital Clínic de Barcelona (protocol code HCB/2017/0519 and date of approval 06/29/2017).

Informed Consent Statement: Written informed consent has been obtained from the patient(s) to publish this paper.

Data Availability Statement: All data generated or analyzed during this study are included in this article. Further enquiries can be directed to the corresponding author.

Acknowledgments: The authors acknowledge the infrastructure and support of the Pathology Unit of Hospital Clínic de Barcelona and specially to Miriam Cuatrecasas and Sandra López-Prades, who

helped us in the sample collection, manipulation, and lesion identification. The authors also want to thank the Universitat Politècnica de Catalunya for letting us have the coaxial probe, and specially to Prof. Joan O'Callaghan for his advice.

Conflicts of Interest: M.G., I.B. and G.F. are shareholders of MiWEndo Solutions. W.D., R.S., A.G., S.M. and L.N. declare no conflict of interest.

References

1. Ferlay J, Ervik M, Lam F, Colombet M, Mery L, Piñeros M. Global Cancer Observatory: Cancer Today. *Lyon Int Agency Res Cancer*. 2020,.
2. Bray F, Ferlay J, Soerjomataram I, Siegel RL, Torre LA, Jemal A. Global cancer statistics 2018: GLOBOCAN estimates of incidence and mortality worldwide for 36 cancers in 185 countries. *CA Cancer J Clin*. 2018,*68*(6); pp.394–424.
3. Surveillance Research Program, National Cancer Institute SEER*Stat software [Internet]. Available from: seer.cancer.gov/seerstat
4. Müller AD, Sonnenberg A. Prevention of colorectal cancer by flexible endoscopy and polypectomy. A case-control study of 32,702 veterans. *Ann Intern Med* [Internet]. 1995 [cited 2017 May 12],*123*(12); pp.904–10. Available from: http://www.ncbi.nlm.nih.gov/pubmed/7486484
5. Winawer SJ, Zauber AG, Ho MN, O'Brien MJ, Gottlieb LS, Sternberg SS, et al. Prevention of Colorectal Cancer by Colonoscopic Polypectomy. *N Engl J Med* [Internet]. 1993 [cited 2017 May 12],*329*(27); pp.1977–81. Available from: http://www.ncbi.nlm.nih.gov/pubmed/8247072
6. van Rijn JC, Reitsma JB, Stoker J, Bossuyt PM, van Deventer SJ, Dekker E. Polyp miss rate determined by tandem colonoscopy: a systematic review. *Am J Gastroenterol*. 2006,*101*(2); pp.343–50.
7. Samadder NJ, Curtin K, Tuohy TM, Pappas L, Boucher K, Provenzale D, et al. Characteristics of missed or interval colorectal cancer and patient survival: a population-based study. *Gastroenterology*. 2014,*146*(4); pp.950–60.
8. Lee T, Rees C, Blanks R, Moss S, Nickerson C, Wright K, et al. Colonoscopic factors associated with adenoma detection in a national colorectal cancer screening program. *Endoscopy* [Internet]. 2014 [cited 2017 May 12],*46*(03); pp.203–11. Available from: http://www.ncbi.nlm.nih.gov/pubmed/24473907
9. East JE, Saunders BP, Burling D, Boone D, Halligan S, Taylor SA. Surface visualization at CT colonography simulated colonoscopy: effect of varying field of view and retrograde view. *Am J Gastroenterol*. 2007,*102*(11); pp.2529–35.
10. Corley AC, Jensen CD, Marks AR, Zhao WK, Lee JK, Doubeni CA, et al. Adenoma Detection Rate and Risk of Colorectal Cancer and Death. *N Engl J Med*. 2014,*370*(1); pp.1298–1306.
11. Ngu WS, Bevan R, Tsiamoulos ZP, Bassett P, Hoare Z, Rutter MD, et al. Improved adenoma detection with Endocuff Vision: The ADENOMA randomised controlled trial. *Gut*. 2019,*68*(2); pp.280–8.
12. Dik VK, Gralnek IM, Segol O, Suissa A, Belderbos TDG, Moons LMG, et al. Multicenter, randomized, tandem evaluation of EndoRings colonoscopy - Results of the CLEVER study. *Endoscopy*. 2015,*47*(12); pp.1151–8.
13. Ngu WS, Rees C. Can technology increase adenoma detection rate? *Therap Adv Gastroenterol*. 2018,*11*; pp.1–18.
14. Kumashiro R, Konishi K, Chiba T, Akahoshi T, Nakamura S, Murata M, et al. Integrated endoscopic system based on optical imaging and hyperspectral data analysis for colorectal cancer detection. *Anticancer Res* [Internet]. 2016,*36*(8); pp.3925–32. Available from: http://ar.iiarjournals.org/content/36/8/3925.full.pdf%0Ahttp://ovidsp.ovid.com/ovidweb.cgi?T=JS&PAGE=reference&D=emexa&NEWS=N&AN=612865834%0Ahttps://www.scopus.com/inward/record.uri?eid=2-s2.0-84991745865&partnerID=40&md5=82910e0290d5c4f4a3ff585e021dea13
15. Ahmad OF, Soares AS, Mazomenos E, Brandao P, Vega R, Seward E, et al. Artificial intelligence and computer-aided diagnosis in colonoscopy: current evidence and future directions. *lancet Gastroenterol Hepatol* [Internet]. 2019 [cited 2018 Dec 14],*4*(1); pp.71–80. Available from: http://www.ncbi.nlm.nih.gov/pubmed/30527583
16. Repici A, Badalamenti M, Maselli R, Correale L, Radaelli F, Rondonotti E, et al. Efficacy of Real-Time Computer-Aided Detection of Colorectal Neoplasia in a Randomized Trial. *Gastroenterology* [Internet]. 2020,*159*(2); pp.512-520.e7. Available from: https://doi.org/10.1053/j.gastro.2020.04.062
17. Nikolova NK. Introduction to Microwave Imaging [Internet]. Cambridge: Cambridge University Press; 2017 [cited 2017 Oct 24]. 366 p. Available from: http://ebooks.cambridge.org/ref/id/CBO9781316084267
18. Shere M, Lyburn I, Sidebottom R, Massey H, Gillett C, Jones L. MARIA® M5: A multicentre clinical study to evaluate the ability of the Micrima radio-wave radar breast imaging system (MARIA®) to detect lesions in the symptomatic breast. *Eur J Radiol* [Internet]. 2019 [cited 2020 Mar 26],*116*; pp.61–7. Available from: https://www.sciencedirect.com/science/article/pii/S0720048X19301512?via%3Dihub
19. O'Loughlin D, O'Halloran M, Moloney BM, Glavin M, Jones E, Elahi MA. Microwave breast imaging: Clinical advances and remaining challenges. *IEEE Trans Biomed Eng*. 2018,*65*(11).
20. Toaha Mobashsher A, Abbosh AM. On-site Rapid Diagnosis of Intracranial Hematoma using Portable Multi-slice Microwave Imaging System. *Nat Publ Gr* [Internet]. 2016 [cited 2017 Nov 22],. Available from: https://www.nature.com/articles/srep37620.pdf

21. Meaney PM, Goodwin D, Golnabi AH, Zhou T, Pallone M, Geimer SD, et al. Clinical microwave tomographic imaging of the calcaneus: a first-in-human case study of two subjects. *IEEE Trans Biomed Eng* [Internet]. 2012 [cited 2017 Oct 24],*59*(12); pp.3304–13. Available from: http://www.ncbi.nlm.nih.gov/pubmed/22829363
22. Semenov SY, Posukh VG, Bulyshev AE, Williams TC, Sizov YE, Repin PN, et al. Microwave Tomographic Imaging of the Heart in Intact Swine. *J Electromagn Waves Appl J Electromagn Waves Appl* [Internet]. 2006 [cited 2017 Oct 24],*207*(7); pp.873–90. Available from: http://www.tandfonline.com/action/journalInformation?journalCode=tewa20
23. Guardiola M, Djafri K, Challal M, Gonzalez Ballester MA, Fernandez-Esparrach G, Camara O, et al. Design and evaluation of an antenna applicator for a microwave colonoscopy system. *IEEE Trans Antennas Propag*. 2019,*67*(8); pp.4968–77.
24. Garrido A, Sont R, Dghoughi W, Marcoval S, Romeu J, Fernández-Esparrach G, et al. Polyp Automatic Detection using Microwave Endoscopy for Colorectal Cancer Prevention and Early Detection. Phantom Validation. *IEEE Access*.
25. Fernández-Esparrach G, Garrido A, Sont R, Dghoughi W, Marcoval S, Cuatrecasas M, et al. Microwave-Based Colonoscopy: Preclinical Evaluation in an Ex Vivo Human Colon Model. *Gastroenterol Res Pract*. 2022,*2022*.
26. Garrido-atienza A, Dghoughi W, Robert JR, Garcia MG. Preliminary phantom-based dynamic calibration techniques assessment for microwave colonoscopy systems. ; pp.6–9.
27. La Gioia A, Porter E, Merunka I, Shahzad A, Salahuddin S, Jones M, et al. Open-Ended Coaxial Probe Technique for Dielectric Measurement of Biological Tissues: Challenges and Common Practices. *Diagnostics*. 2018,*8*(2); pp.40.
28. Guardiola M, Buitrago S, Fernández-Esparrach G, O'Callaghan JM, Romeu J, Cuatrecasas M, et al. Dielectric properties of colon polyps, cancer, and normal mucosa: Ex vivo measurements from 0.5 to 20 GHz. *Med Phys*. 2018,*45*(8); pp.3768–82.
29. Shlepnev Y. Evaluation of S-Parameters Similarity with Modified Hausdorff Distance. *EPEPS 2021 - IEEE 30th Conf Electr Perform Electron Packag Syst*. 2021,.
30. Zamani A, Abbosh A. Hybrid Clutter Rejection Technique for Improved Microwave Head Imaging. *IEEE Trans Antennas Propag*. 2015,*63*(11); pp.4921–31.
31. Brutlag JD. Aberrant behavior detection in time series for network monitoring. *Proc 14th Conf Syst Adm LISA 2000*. 2000,; pp.139–46.
32. Ward A, Glynn P, Richardson K. Internet service performance failure detection. *Perform Eval Rev*. 1998,*26*(3); pp.38–43.